DOI: 10.13009/EUCASS2017-605

7TH EUROPEAN CONFERENCE FOR AERONAUTICS AND AEROSPACE SCIENCES (EUCASS)

DOI: ADD DOINUMBER HERE

Large Eddy Simulation of Flow and Combustion in a Single-Element GCH_4/GOX Rocket Combustor

D. Maestro⋆†*, B. Cuenot*⋆ *and L. Selle*§

⋆*CERFACS*
42 Avenue Gaspard Coriolis, 31057 Toulouse Cedex 01, France

§*Institut de Mécanique des Fluides de Toulouse (IMFT) - Université de Toulouse, CNRS-INPT-UPS*
2 Allée du Professeur Camille Soula, 31400 Toulouse, France

maestro@cerfacs.fr · cuenot@cerfacs.fr · laurent.selle@imft.fr

†Corresponding author

Abstract

A single element GCH_4/GOx rocket combustion chamber has been computed, via Large Eddy Simulation of the experimental combustion rig developed at the Technische Universität München. The aim of this work is to validate the capability of the AVBP solver for such conditions as well as to analyse the flow and combustion features at high pressure. A particular focus is set on the prediction of wall heat flux, a key point for the development of reusable engines. Longitudinal distribution of wall heat flux, as well as chamber pressure, have been plotted against experimental data. Results have been analysed in order to point out the main requirements to obtain a good evaluation of the wall heat flux with this simulation framework.

1. Introduction

Over the past ten to fifteen years, the market of access to space has significantly shifted from government agencies to the private sector. This new paradigm calls for increased cost effectiveness and there are claims that the cost per kilogram into orbit could be reduced by more than one order of magnitude. Such ambitious goals require important changes in the propulsion system, among which the use of reusable engines and storable fuel. For these reasons, hydrocarbons, and specifically methane are potential substitutes for hydrogen, which is commonly used today. The characteristics of methane are particularly promising: a high specific impulse (compared to kerosene for instance), favorable cooling properties, high density at common tank pressures, low pollution and low cost both for production and handling.[1] Given the objective of reusable engines, the accurate prediction of wall temperature during operation is mandatory. Consequently, the development of accurate numerical methodologies for the determination of heat transfer in combustion chambers is a subject of major interest. There is a lack of knowledge of CH_4/O_2 combustion at high pressure and numerical simulations can contribute to the understanding of the physical phenomena and predict the thermal stress on the chamber walls. The aim of this work is to analyse the flow and combustion dynamics of a single-element GCH_4/GOx rocket combustion chamber, via the Large-Eddy Simulation (LES) of the experimental setup of Celano et al.,[2] for which experimental data is available.

This test case has been firstly simulated during the 2015 SFB/TRR 40 Summer Program. A "blind test" was performed by different groups, showing a significant spread in results, compared to the test data.[3,4] Updated results have been presented by Roth et al.,[5] Maestro et al.[6] and Müller et al.[7]

These works demonstrated the capability of the AVBP code to perform such a type of calculation and highlighted the need to correctly solve the flame dynamics and the wall flow to have a good estimation of the heat flux. The aim of the present paper is to show recent progress in the simulation of the test case, performing a full 3D LES of the test facility, as a new step to achieve the correct wall heat flux evaluation.

The paper is structured as follows: first, the experimental setup is presented in section 2, then simulation strategy and numerical setup are described in section 3. Flow and flame structures are analyzed in section 4, where quantitative

DOI: 10.13009/EUCASS2017-605

results are shown. Finally, conclusions and future works are summarised in section 5.

2. Experimental configuration

The configuration, which is schematically reported in Fig. 1, consists of a single shear coaxial injector feeding a 290 mm-long combustion chamber, operating at a nominal pressure of 20 bar. The injector is flush mounted on an oxygen-free copper combustion chamber with a square cross section (12 × 12 mm) and a nozzle at the exit, see Tab. 1. Sonic orifices determine the inlet mass flow rates of $\dot{m}_{CH4} = 0.0017$ kg/s and $\dot{m}_{O2} = 0.0045$ kg/s, respectively. No

Table 1: Characteristic combustion chamber and injector dimensions.

Combustion chamber			**Injector**		
Chamber length	[mm]	290	GOx diameter	[mm]	4
Chamber width	[mm]	12	GOx post wall thickness	[mm]	0.5
Chamber height	[mm]	12	GOx post recess	[mm]	0
Throat height	[mm]	4.8	GCH_4 outer diameter	[mm]	6
Contraction ratio A_{cc}/A_{th}	[-]	2.5	Injector area ratio A_{GCH4}/A_{GOx}	[-]	0.7

cooling system is present and therefore the wall chamber temperature increases during the burning experimental time, which is of 3 s. The measured wall temperature in the chamber is averaged over a shorter evaluation time of 0.5 s, centred at 2/3 of the burning time. Measurements of the axial evolution of chamber pressure and wall heat flux are reported in Celano et al.[2]

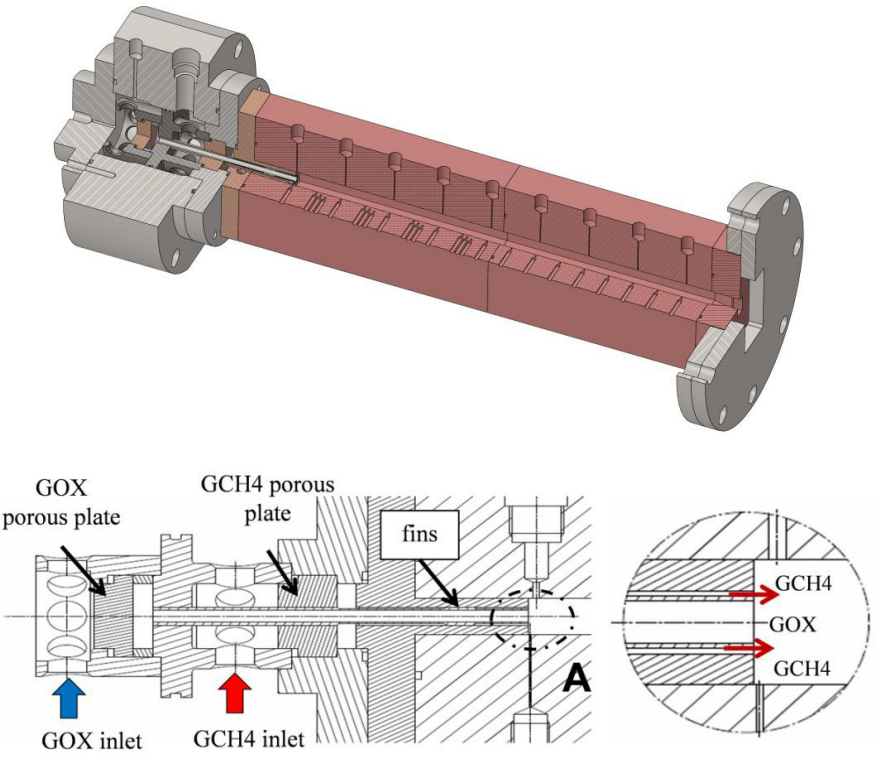

Figure 1: Single-injector combustion chamber and detail of the injector.

DOI: 10.13009/EUCASS2017-605

3. Simulation setup

Geometry - Computational domain and mesh characteristics

The computational domain is the full three-dimensional chamber, starting 1 *mm* before the faceplate, so that only a small part of the injector is calculated. The computational domain extends to the nozzle exit and the full nozzle is simulated. The computational domain is discretized with a fully tetrahedral unstructured mesh of about 130 million cells. Particular attention has been put on the flame zone refinement, especially in the post-tip zone, which has been discretized with 20 cells. A schematic view of the mesh in the near injector region is presented in Fig. 2.

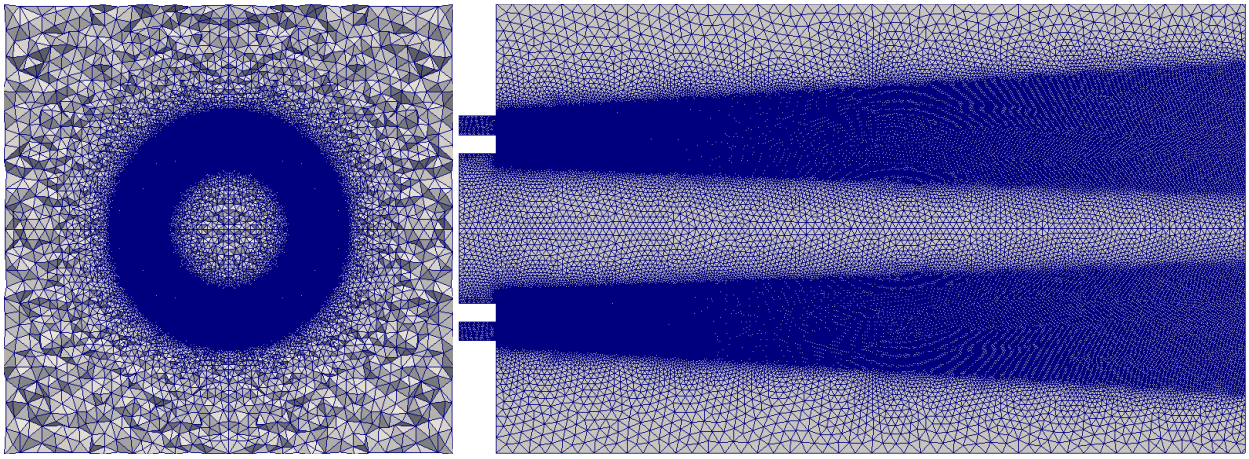

Figure 2: Left: transverse cut through the mesh 2 mm downstream of the injection plane. Right: longitudinal cut through the mesh near the injector.

Boundary conditions

Gaseous oxygen (GOx) and methane (GCH_4) mass flow rates have been prescribed at inlet, as well as the experimentally measured temperature, using the NSCBC formulation.[8] At the outlet, the flow is expected to be supersonic, therefore there is no need to specify any boundary condition. The velocity profile prescribed at inlet corresponds to a turbulent flow, coherent with a previous RANS simulation.[9] The injectors walls, as well as the faceplate, post-tip and nozzle walls are treated as adiabatic walls, with a law-of-the-wall formalism. Chamber walls are modeled with isothermal wall laws, using an improved formulation that couples the velocity and temperature profiles to take into account the interaction between the strong temperature and velocity gradients in the boundary layer. A detailed description of this coupled wall law can be found in the work of Cabrit.[10] The imposed temperature profile, taken from Celano et al.,[2] is obtained by averaging the temperatures measured on the upper and lateral walls. In the simulation the same temperature profile has been imposed on the four walls.

Numerical setup

The AVBP solver, developed by CERFACS and IFPEN, is used to carry out the LES. It is an unstructured, explicit, compressible code.[11,12] The second order in time and space Lax-Wendroff[13] numerical scheme is used. The subgrid stress tensor is closed using the Sigma model.[14] Thermal and species diffusion terms at the subgrid level are deduced assuming an eddy-diffusivity approach assigning constant turbulent Prandtl number and turbulent Schmidt number (value fixed at 0.7 for both). Regarding turbulence/combustion interaction, the flame/eddies interaction is fully resolved on the grid and no additional model is needed. A power-law function is used to model the molecular viscosity and a constant Prandtl number is used for the thermal conductivity.

$$\mu = \mu_{ref}\left(\frac{T}{T_{ref}}\right)^n, \quad \lambda = \frac{\mu\, c_p}{\mathrm{Pr}} \tag{1}$$

The coefficients in the model have been fitted to the results of the Chapman-Enskog theory, $\mu_{ref} = 1.282 \times 10^{-5}$ Pa $\cdot$ s, $n = 0.703$ and $\mathrm{Pr} = 0.895$. The reference temperature is $T_{ref} = 278$ K and c_p denotes the heat capacity at constant pressure.

DOI: 10.13009/EUCASS2017-605

Chemical kinetics

The LES is run with the analytically reduced mechanism developed by Sankaran et al.[15] Analytical mechanisms use a quasi-steady-state (QSS) approximation for some species and a partial equilibrium formulation for some reactions. The quasi-steady-state approach can be used when the creation rate of a species is slow compared to its consumption rate, which means that the species is very quickly consumed after being produced so that its mass can not significantly change. In this case the net rate of the species is considered equal to zero and its concentration is calculated from an analytical formulation instead of its conservation equation, which is not solved. Partial equilibrium hypothesis is valid when both the forward and backward reaction rates of a species are fast compared to all other reactions.
This analytical mechanism has been derived for air/methane lean premixed combustion through the sequential application of directed relation graph (DRG),[16] sensitivity analysis and computational singular perturbation (CSP)[17] over the GRI-1.2 detailed mechanism.[18] The final skeletal mechanism contains 73 elementary reactions with 17 species, among which CH_2, $CH_2(S)$, HCO and CH_2OH are identified as QSS species through CSP. The remaining 13 species are fully resolved, namely, H_2, H, O, O_2, OH, H_2O, HO_2, CH_3, CH_4 , CO, CO_2, CH_2O and N_2. The QSS algebraic relations are solved analytically.
It has been demonstrated by Mari et al.[19] that oxy-combustion of methane is quite sensitive to the number of species used in the reduced mechanism and how, if they are not sufficient, the equilibrium state of the burnt gases is not correctly retrieved. For this reason the chemical scheme has been validated first on equilibrium calculations and then on 1D premixed and strained counterflow diffusion flames with representative strain rate values. This has been done using the CANTERA[20] software and a detailed analysis can be found in Maestro et al.[6]

4. Results and discussion

In this section results of the LES are presented. A first part deals with an extensive investigation of needs in terms of setup to correctly retrieve the flow and flame shape in such a configuration. The focus is set on the importance of having sufficient flame and flow resolution in the near-injection region. An analysis of the flame features follows, with a qualitative and quantitative description of the actual GCH_4/GOx flame structure and dynamics. Finally a quantitative analysis of the axial evolution of the chamber pressure and wall heat flux is shown.

Near injector dynamics and resolution requirements

The physical mechanisms at play closely downstream of the injection plane (in the post-tip zone) have been found to be of leading order for the overall flow and flame dynamics. To highlight the importance of the correct modeling of these phenomena, results of the present numerical setup are compared with preliminary ones obtained on a coarser mesh in Fig. 3. The upper half of each subfigure corresponds to the coarse mesh, where the post-tip zone is discretised with 10 points and the mesh is rapidly coarsened downstream. The lower half corresponds to the present mesh (cf. Fig. 2), in which the post-tip zone is discretised with 20 points and the resolution is kept for more than one injector diameter. This change by a factor of two in the resolution, drastically changes the flow and flame structure downstream of the post-tip.

On the top row of Fig. 3, left side, instantaneous fields of axial velocity are presented. It can be seen how several recirculation zones appear (the white isoline represents the zero axial velocity), depending on the mesh used: a "tip recirculation zone" (fine mesh) in the post-tip zone, a "central recirculation zone" (coarse mesh) a little further downstream and "corner recirculation zones" in the chamber corners (both meshes). One can immediately notice how in the case of the coarse mesh the "tip recirculation zone" almost disappears. On the contrary, this recirculation zone, filled with hot burnt gases, clearly appears with the fine mesh and its presence is crucial for the flow structure just downstream: the reactant jets are pushed one against the other by this vortical structure, they mix and do not leave place for any "central recirculation zone" downstream.

As a consequence of this difference in flow structure, the flame structure is modified too. Differences can be seen in the top row of Fig. 3, right side, where instantaneous temperature fields are presented. With the coarse mesh, the flame is less strained and burnt gases expand radially. Using a fine mesh induces higher strain on the flame which remains very thin.

These differences in flame structure have in turn an impact on the flow structure: through radial expansion, the thick flame on the coarse mesh pushes the CH_4 jet toward the chamber walls, while the thin flame on the fine mesh does not lead to sufficient expansion to modify the flow. The jet breakdown position coincides in this case with a slowdown zone, but no back flow is observed. The "corner recirculation zone" length is also affected by this change in flow topology, changing from 9 *mm* with the coarse mesh to 14 *mm* with the fine one.

DOI: 10.13009/EUCASS2017-605

Flame stabilization is also strongly affected by the flow structure downstream the post-tip, as can be seen on the bottom row of Fig. 3, where fields of instantaneous heat release rate are shown. With the coarse mesh the reactants quickly diffuse at the post-tip creating favorable conditions for combustion and leading to a large local heat release rate. On the contrary, with the fine mesh, the recirculation zone confines the flame on the oxygen side and dilutes the CH_4 flux with burnt gases, limiting the heat release rate, which reaches its maximum further downstream. In both cases the maximum of heat release rate is aligned with the isoline of stoichiometric mixture fraction, indicating that combustion occurs in the diffusion regime, which will be further discussed.

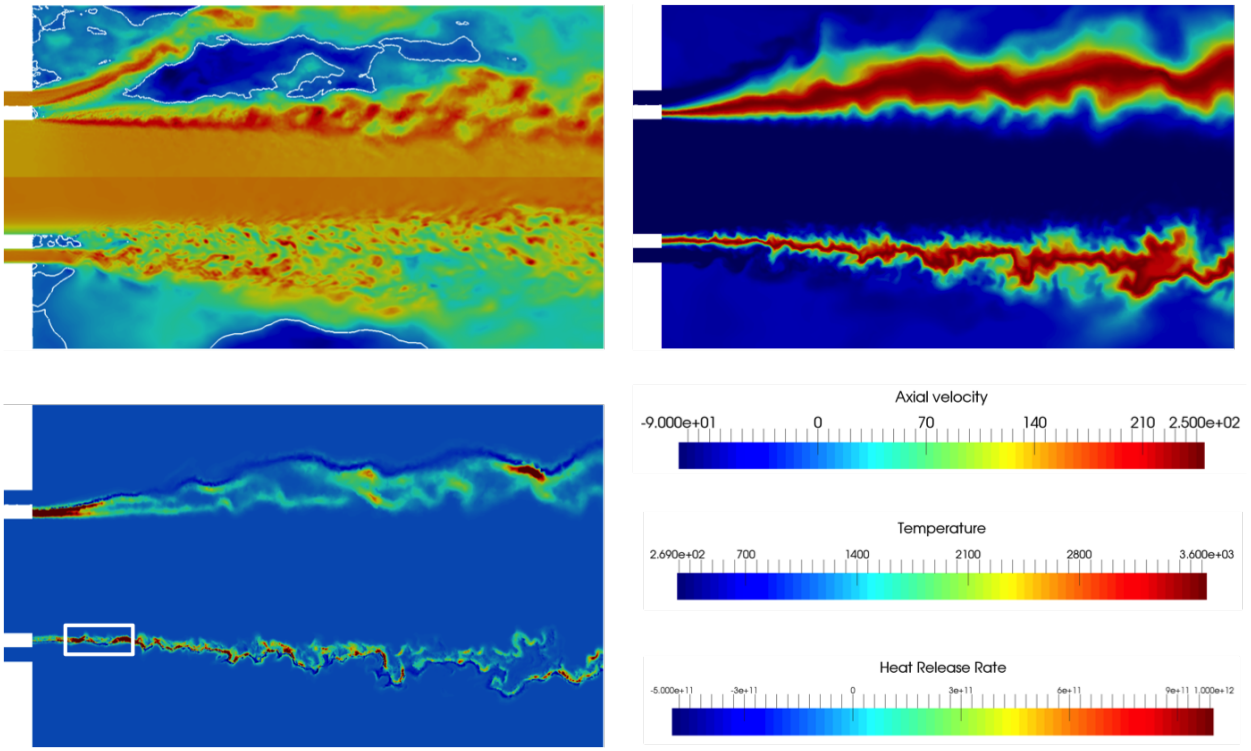

Figure 3: Longitudinal cuts of instantaneous fields in the near-injection region. Upper half: coarse mesh; lower half: fine mesh. Top row, left: axial velocity. Top row, right: temperature. Bottom row: heat release rate.

Figure 4 shows a comparison of the instantaneous temperature fields in a region extending further downstream, up to one third of the chamber length. This points out two main effects that have to be taken into account, especially if the aim is to evaluate heat fluxes at walls. The first thing to underline is how the flow and flame dynamics in the near injection region strongly affects the overall flame shape. On the coarse mesh the flame, which immediately thickens in the post-tip region (as seen in Fig. 3), remains thick downstream since the resolved flow is not capable to strain it highly, leading to an early convection of hot gases towards the wall. This phenomenon is not visible for the fine mesh, where a thin flame is kept due the high strain imposed by the flow. Hot gases reach the wall zone much further downstream. The second effect one can notice from Fig. 4 is how important it is to keep a good flame resolution also

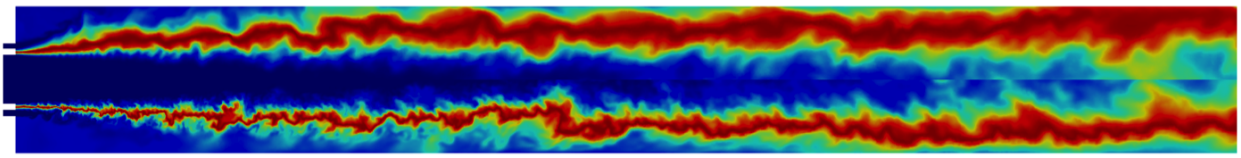

Figure 4: Longitudinal cut of instantaneous temperature field over one third of the chamber length. Top: coarse mesh; bottom: fine mesh.

far away from the injection plane. In such a strongly confined configuration the walls are be close to the flame zone; knowing that in the diffusion regime the flame adapts its thickness to the mesh size, a coarse mesh can lead to a flame which touches the walls, leading therefore to a completely wrong estimation of the flame shape and wall heat flux. In the present configuration, the flame on the fine mesh has been found indeed to never touch the walls and to close at nearly two thirds of the chamber.

DOI: 10.13009/EUCASS2017-605

Mean flame shape

The time-averaged fields of temperature (Fig. 5) and CH_4 mass fraction (Fig. 6) are now analysed. It can be seen in Fig. 5 that the flame is stabilised by a recirculation zone of hot gases between the oxidiser and fuel streams, downstream the post-tip. From there the mean reaction zone thickens and the flame broadens towards the downstream end of the combustor. The maximum temperature reached by the flame is 3405 K, close to the adiabatic temperature predicted by CEA[21] (3444 K), denoting a good behaviour of the kinetic scheme. On the bottom row of Fig. 5 one can notice how in the near injection region, the flame shape is imposed by the injectors geometry, leading to a cylindrical flame. Further downstream, the flow field is dominated by the turbulent mixing and the flame shape tends to adapt to the square section of the chamber.

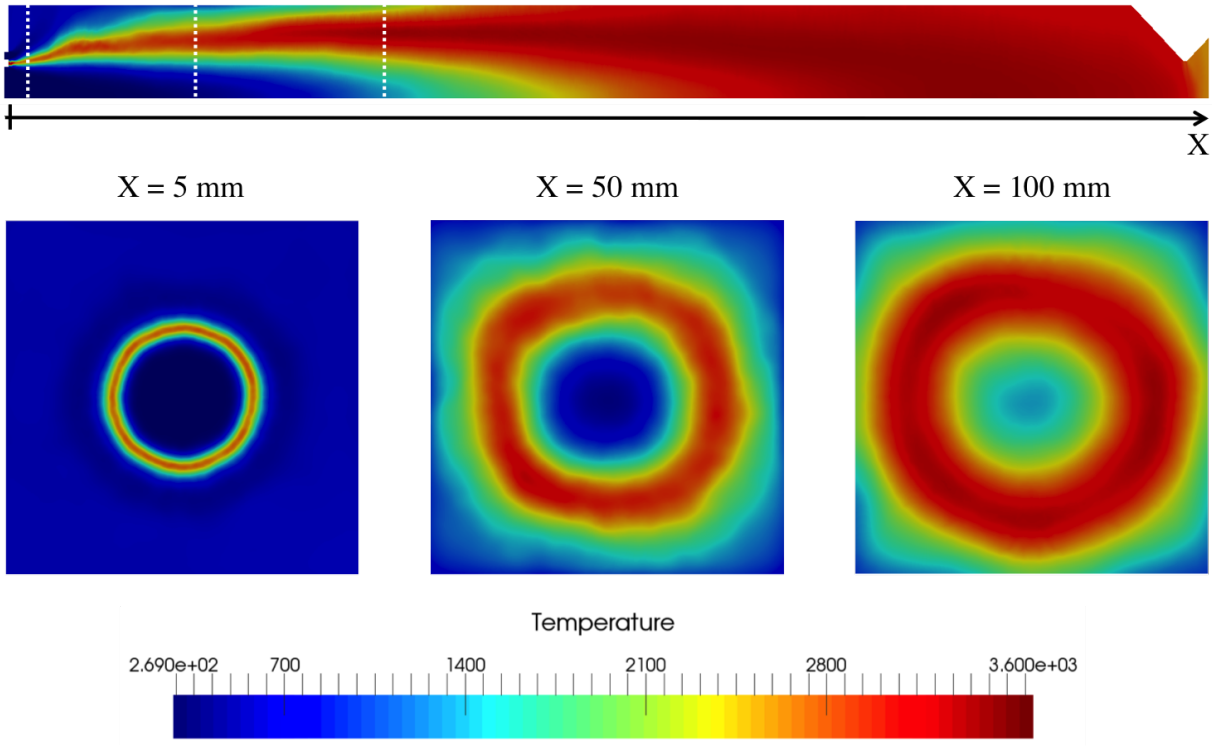

Figure 5: Top row: longitudinal cut of mean temperature field (stretched by a factor of 4 in y-direction). Bottom row: transverse cuts of mean temperature fields at three different axial positions.

The fields of methane mass fraction presented in Fig. 6 show that the edges of the chamber are filled with CH_4, and remain significantly colder than the central region of the chamber walls. This has been found to have a noticeable impact on the circumferential distribution of the heat flux at walls, as shown below. The top rows of Figs. 5 and 6 also show that a thermal boundary layer is formed due to the joint effects of heat losses, induced by the constant-temperature boundary condition, and the presence of a layer of cold methane near the walls. The thermal boundary layer is less and less visible downstream due to the preferential concentration of methane at the edges. A thin layer is still present it is not visible with the colour scale used here.

This analysis provides key information on the flow and flame dynamics in such a configuration, pointing out how multiple mechanisms have to be taken into account if one wants to perform a correct wall heat flux evaluation. The wall heat flux is influenced indeed both by the temperature gradient and the thermal conductivity (gas composition) at walls. The temperature gradient is obviously related to the local gas temperature, which has to be well predicted by the flame dynamics and by the flow convection as shown previously. It is not to be forgotten how the correct estimation of the temperature gradient is also due to the accuracy of the wall-law model and on the grid resolution at walls (namely the value of y^+). This is not addressed in the present paper but has already been studied and is the subject of ongoing work. Moreover, the gas composition at walls is driven by the kinetic mechanism and flow topology. Indeed a correct gas composition has to be retrieved in regions close to the walls, where radical species can also sustain exothermic or endothermic chemical reactions. For example HO_2 is involved in low-activation energy reactions, which are favoured near walls where the mixture is cooled down. The cooling of burnt gas near walls may also slow down the CO oxidation.

DOI: 10.13009/EUCASS2017-605

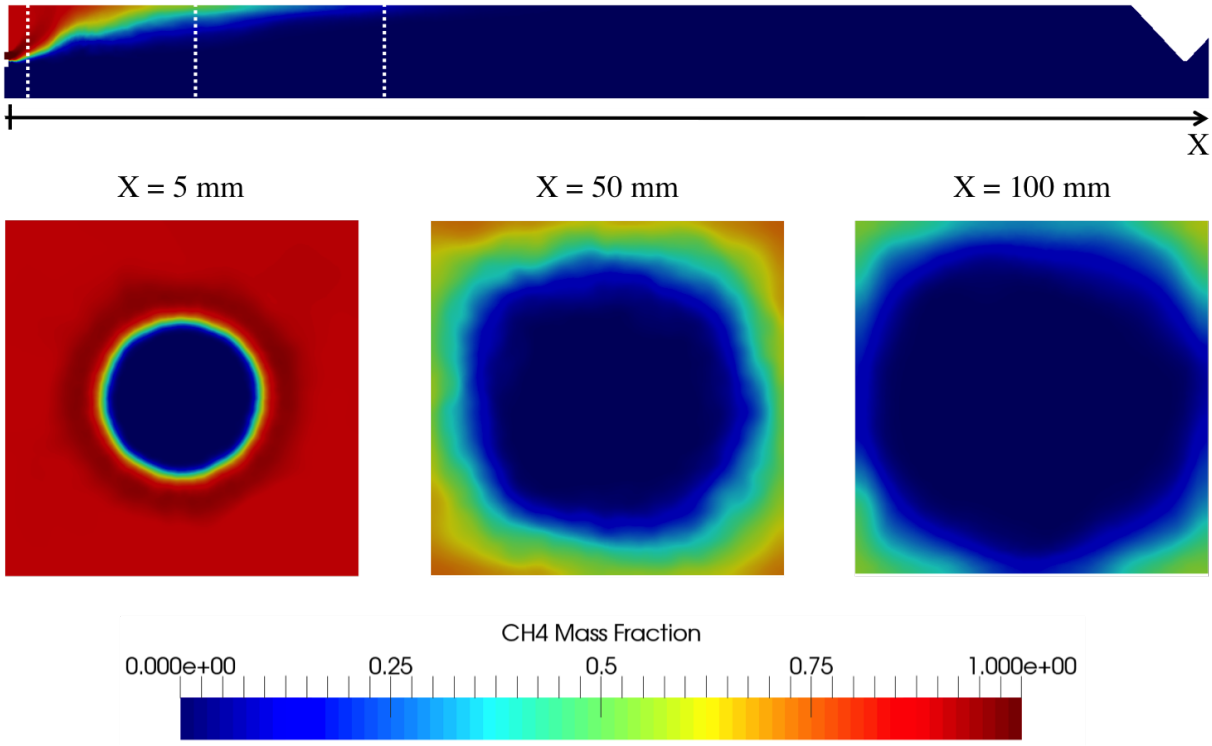

Figure 6: Top row: longitudinal cut of mean methane mass fraction field (stretched by a factor of 4 in y-direction). Bottom row: transverse cuts of mean methane mass fraction fields at three different axial positions.

Flame structure

Figure 7 shows an instantaneous field of mixture fraction in the whole chamber, calculated according to Bilger's definition.[22] The isoline of stoichiometric mixture fraction (white line) has been taken as an indicator of the flame position since the flame burns in a diffusion regime. As it can be seen the flame closes at nearly two thirds of the chamber length, and does not interact with the walls.

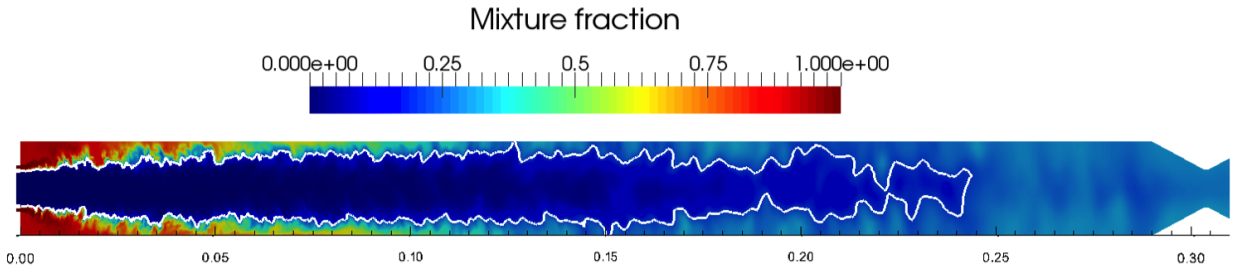

Figure 7: Field of mixture fraction in a plane perpendicular to injection. White line: isoline of stoichiometric mixture fraction. Horizontal axis: distance from the faceplate in *m*. View is stretched by a factor of 2 for visualization reasons.

In order to confirm that the combustion regime is indeed diffusion, the flame structure in the 3D simulation has been compared to a 1D counterflow diffusion flame. Values for the 3D simulation have been collected in the vicinity of the injector, between 1 and 3 *mm* downstream the post-tip end, in a cylinder around the flame (white box in Fig. 3). The 1D flame calculation has been performed with the Cantera software at a representative scalar dissipation rate along the stoichiometric surface $\chi_s = 2D(\partial z/\partial x_i)_s^2$, where z the mixture fraction and D the diffusion coefficient have been extracted from the simulation. Results are reported in Fig. 8. A classical diffusion flame structure at strain rates far from extinction can be identified. The LES simulation exhibits some dispersion, due to the range of resolved strain rates. Note that the maximum flame temperature is reached and that there is no evidence of any significant effect of heat losses on the flame structure.

DOI: 10.13009/EUCASS2017-605

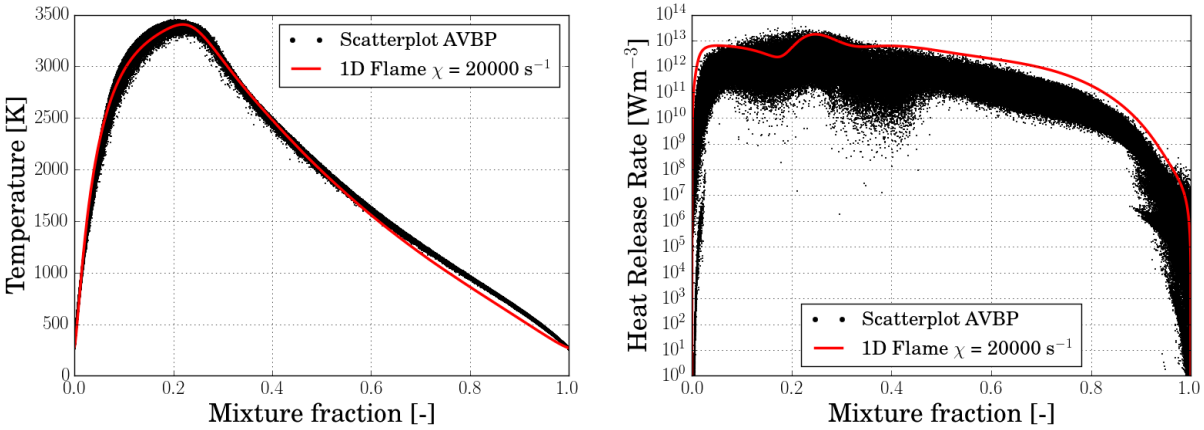

Figure 8: Scatterplots vs mixture fraction in the near injection zone, with superimposed curve for a 1D counterflow diffusion flame at a characteristic scalar dissipation rate value. Left: temperature; right: heat release rate (logarithmic scale).

Comparison with the experiment

The available experimental data for pressure distribution and heat flux at the chamber wall allow for a quantitative comparison between the LES results and the experimental measurements. Figure 9 shows the time-averaged pressure distribution along the chamber axis. In order to better compare the shape of the curves, the normalized pressure profiles are also presented, using the value at the location of the last pressure transducer in the experiment, i.e., at x = 272.5 *mm*, as a reference. The profile extracted from experimental measurements shows a fast pressure increase close to the injector, followed by a constant and relatively slow pressure decrease. The pressure difference between the two measurement positions at the end of the chamber is nearly zero, indicating the end of the combustion process.

The comparison with the LES results shows that the overall pressure level is quite well predicted, with a slight overestimation. Looking at the normalised profiles, right side of Fig. 9, one can notice how in the first half of the chamber the decrease in pressure is slightly too fast, denoting a higher heat release rate than in the experiment. However, close to the end of the chamber, the pressure slope decreases, indicating a reduction in heat release and the end of combustion, consistently with the experiment. This is also in agreement with the flame closure at nearly two thirds of the chamber observed in Fig. 7.

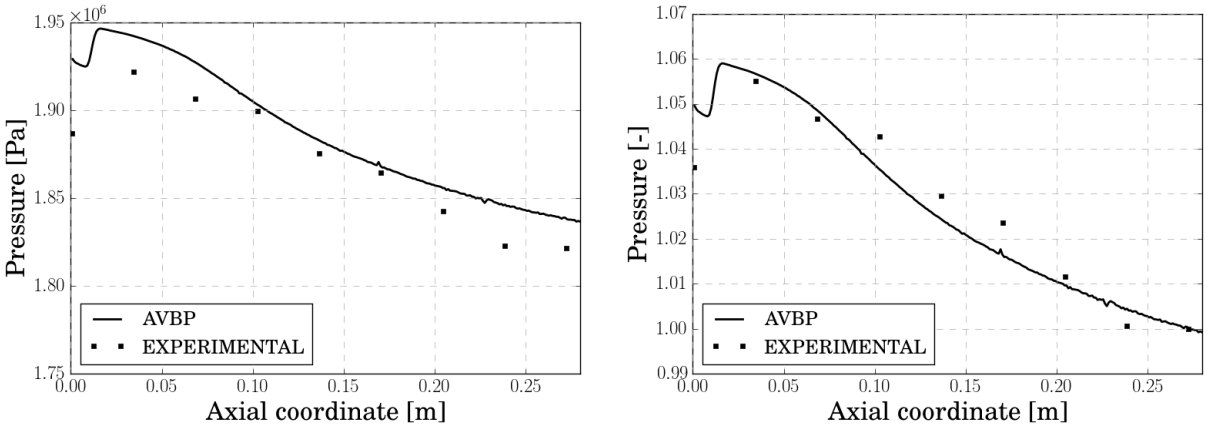

Figure 9: Left: time averaged axial pressure evolution. Right: time averaged normalized pressure evolution

During the hot fire tests, the temperature along the center of the chamber walls has been recorded. Using this data, Celano et al.[2] reconstructed the wall heat flux by solving an inverse heat conduction problem. The main assumption of these calculations is that the heat flux is constant in the circumferential direction of the chamber. In order to compare the LES data with the experimental heat flux profile, the numerical data have been therefore circumferentially averaged

DOI: 10.13009/EUCASS2017-605

too. Results are presented in Fig 10 (left). Experimental data show a local maximum of heat flux in the near injection region, as a result of the recirculation zone. Downstream the heat flux increases with a fairly constant rate, reaching the highest heat load of 5.33 MW/m^2 at the end of the chamber. The numerical simulation predicts fairly well the axial evolution of the wall heat flux, denoting a correct prediction of the flow and flame dynamics. However the values are slightly underestimated in the recirculation zone and overestimated in the rest of the chamber. This is due to the insufficient mesh refinement at walls. Indeed, the mean value of y+ = 1200 is far too large for an accurate evaluation with wall laws. A simulation with a refined mesh at the walls, corresponding to a mean y+ = 40, is underway.

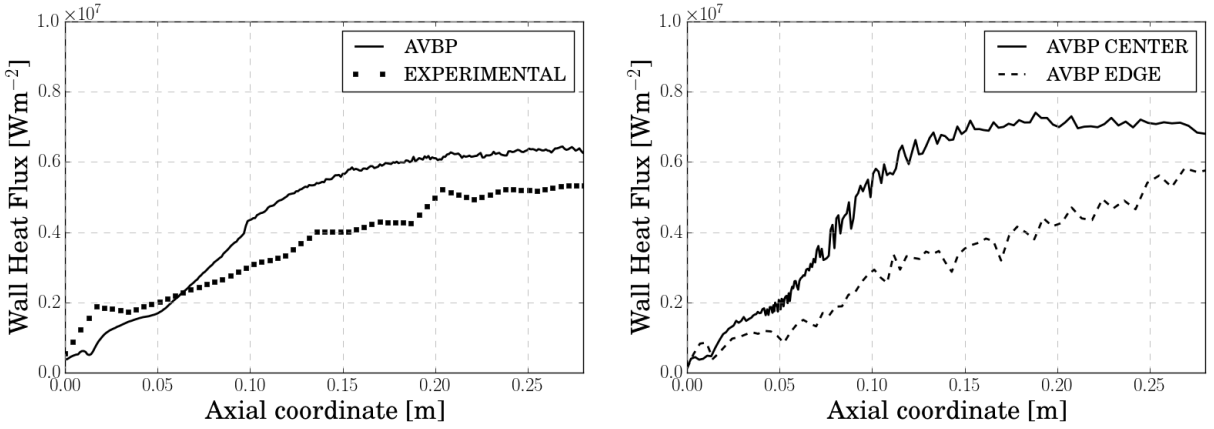

Figure 10: Left: circumferentially averaged axial profiles of heat flux at walls. Right: axial profile of wall heat flux at the chamber center and edge.

In order to verify the assumption of constant heat flux in the circumferential direction, Fig. 10 (right) compares the heat flux along the center of the chamber wall and along the chamber edge. Results show significant differences due to typical features of a round flame in a square section chamber. The preferential convection of fresh methane towards the chamber edges leads to a thicker thermal layer in this zone and so a lower heat flux. On the contrary at the center of the chamber walls, the hot gases are closer, leading to a higher heat flux. A high variability is found between center and edge values. Taking heat flux values in one or the other location will lead to a too strong variation, justifying the need to use circumferentially averaged values in order to compare with reconstructed values from the experiment.

5. Conclusions and future work

A single element GCH_4/GOx rocket combustion chamber has been computed using Large Eddy Simulation. The numerical set-up and the models required to correctly predict the flow and flame dynamics have been presented and the flame structure has been analysed. In particular a high sensitivity to the resolution close to the injector has been found. In addition the flame must be sufficiently solved in order to avoid too fast opening due to numerical diffusion. Numerical simulation data have been compared to experiment, showing and overall good agreement and highlighting the need for better resolution at chamber walls in order to correctly apply wall-laws and recover the wall heat flux. Therefore, it appears that the prediction of wall heat flux in a rocket chamber type configuration requires simultaneous correct modeling of the flow and flame, including the chemical flame structure, the gas composition and the temperature gradient at walls. Work is still ongoing to apply mesh refinement at walls, as a final step to achieve an accurate prediction of the wall heat flux and pressure axial profiles.

6. Acknowledgments

Financial support has been provided by the German Research Foundation (Deutsche Forschungsgemeinschaft - DFG) in the framework of the SFB/TRR 40.
The authors acknowledge CINES of GENCI for giving access to HPC ressources under the allocation 2017-A0012B07036.
The authors extend special thanks to Mariella Celano, Simona Silvestri, Christoph Kirchberger and Gregor Schlieben for providing the test case and insightful discussions.

DOI: 10.13009/EUCASS2017-605

References

[1] D Preclik, G Hagemann, O Knab, C Mading, D Haeseler, Oskar Haidn, A Woschnak, and M DeRosa. Lox-hydrocarbon preparatory thrust chamber technology activities in germany. In *41st AIAA/ASME/SAE/ASEE Joint Propulsion Conference & Exhibit*, 2005.

[2] M. P. Celano, S. Silvestri, G. Schlieben, C. Kirchberger, O. J. Haidn, T. Dawson, R. Ranjan, and S. Menon. Experimental and numerical investigation of GOX-GCH4 shear-coaxial injector element. In *SP-2014-2969417*, 2014.

[3] C. Roth, O. Haidn, H. Riedmann, B. Ivancic, D. Maestro, B. Cuenot, L. Selle, Y. Daimon, A. Chemnitz, R. Keller, et al. Comparison of different modeling approaches for CFD simulations of a single-element GCH4/GOX rocket combustor. *Proceedings of the 2015 Summer Program*, 2015.

[4] D. Maestro, L. Selle, and B. Cuenot. Thermally chained LES of a GCH4/GOX single element combustion chamber. *Proceedings of the 2015 Summer Program*, 2015.

[5] C. Roth, O. Haidn, A. Chemnitz, T. Sattelmayer, G. Frank, H. Müller, J. Zips, R. Keller, P. Gerlinger, D. Maestro, L. Selle, B. Cuenot, and H. Riedmann. Numerical investigation of flow and combustion in a single element gch4/gox rocket combustor. In *52nd AIAA/SAE/ASEE Joint Propulsion Conference*, 2016.

[6] D. Maestro, B. Cuenot, A. Chemnitz, T. Sattelmayer, C. Roth, O. Haidn, Y. Daimon, R. Keller, P. M Gerlinger, G. Frank, et al. Numerical investigation of flow and combustion in a single-element gch4/gox rocket combustor: Chemistry modeling and turbulence-combustion interaction. In *52nd AIAA/SAE/ASEE Joint Propulsion Conference*, 2016.

[7] H. Müller, J. Zips, M. Pfitzner, D. Maestro, B. Cuenot, S. Menon, R. Ranjan, P. Tudisco, and L. Selle. Numerical investigation of flow and combustion in a single-element gch4/gox rocket combustor: A comparative les study. In *52nd AIAA/SAE/ASEE Joint Propulsion Conference*, 2016.

[8] T. Poinsot and S. Lele. Boundary conditions for direct simulations of compressible viscous flows. *J. Comput. Phys.* , 101(1):104–129, 1992.

[9] Y. Daimon, H. Terashimay, Negishi H., and O. Haidn. Combustion Modeling Study for a GCH4/GOX single element combustion chamber: Steady State Simulation and Validations. *Proceedings of the 2015 Summer Program*, 2015.

[10] O. Cabrit. *Modelisation des flux parietaux sur les tuyeres des moteurs a propergol solide*. PhD thesis, 2009.

[11] T. Schønfeld and M. Rudgyard. Steady and unsteady flows simulations using the hybrid flow solver avbp. *AIAA Journal* , 37(11):1378–1385, 1999.

[12] N. Gourdain, L. Gicquel, G. Staffelbach, O. Vermorel, F. Duchaine, J-F. Boussuge, and T. Poinsot. High performance parallel computing of flows in complex geometries - part 2: applications. *Comput. Sci. Disc.*, 2(1):28pp, 2009.

[13] P. D. Lax and B. Wendroff. Systems of conservation laws. *Commun. Pure Appl. Math.* , 13:217–237, 1960.

[14] F. Nicoud, H. Baya Toda, O. Cabrit, S. Bose, and J. Lee. Using singular values to build a subgrid-scale model for large eddy simulations. *Phys. Fluids* , 23(8):085106, 2011.

[15] R. Sankaran, E. Hawkes, J. Chen, T. Lu, and C. Law. Structure of a spatially developing turbulent lean methane–air bunsen flame. *Proceedings of the combustion institute*, 31(1):1291–1298, 2007.

[16] T. Lu and C. Law. A directed relation graph method for mechanism reduction. *Proceedings of the Combustion Institute*, 30(1):1333–1341, 2005.

[17] T. Lu, Y. Ju, and C. Law. Complex csp for chemistry reduction and analysis. *Combustion and Flame*, 126(1):1445–1455, 2001.

[18] M. Frenklach, H. Wang, M. Goldenberg, G.P. Smith, and D.M. Golden. Gri-mech: An optimized detailed chemical reaction mechanism for methane combustion. topical report, september 1992-august 1995. Technical report, SRI International, Menlo Park, CA (United States), 1995.

DOI: 10.13009/EUCASS2017-605

[19] R. Mari. *Influence of heat transfer on high pressure flame structure and stabilization in liquid rocket engines*. PhD thesis, 2015.

[20] D. Goodwin, H. K Moffat, and R. Speth. Cantera: An object-oriented software toolkit for chemical kinetics, thermodynamics, and transport processes. *Caltech, Pasadena, CA*, 2009.

[21] NASA Computer program CEA (Chemical Equilibrium with Applications). `https://www.grc.nasa.gov/WWW/CEAWeb/`.

[22] R.W. Bilger, S.H. Staarner, and R.J. Kee. On reduced mechanisms for methane-air combustion in nonpremixed flames. *Combustion and Flame*, 80(2):135–149, 1990.